Journal of Alloys and Compounds 509 (2011) 512–517

Contents lists available at ScienceDirect

Journal of Alloys and Compounds

journal homepage: www.elsevier.com/locate/jallcom

Effect of addition of $Ba(W_{0.5}Cu_{0.5})O_3$ in $Pb(Mg_{1/3}Nb_{2/3})O_3$–$Pb(Zn_{1/3}Nb_{2/3})O_3$–$Pb(Zr_{0.52}Ti_{0.48})O_3$ ceramics on the sintering temperature, electrical properties and phase transition

Xiaolian Chao [a,b], Zupei Yang [a,b,*], Lirong Xiong [a,b], Zhao Li [a,b]

[a] Key Laboratory for Macromolecular Science of Shaanxi Province, Xi'an 710062, Shaanxi, PR China
[b] School of Chemistry and Materials Science, Shaanxi Normal University, Xi'an 710062, Shaanxi, , PR China

ARTICLE INFO

Article history:
Received 2 May 2010
Received in revised form
10 September 2010
Accepted 18 September 2010
Available online 24 September 2010

Keywords:
Ceramics
Sintering
Piezoelectricity
X-ray diffraction

ABSTRACT

In this work, we report on the $Pb(Mg_{1/3}Nb_{2/3})O_3$–$Pb(Zn_{1/3}Nb_{2/3})O_3$–$Pb(Zr_{0.52}Ti_{0.48})O_3$ (PMN–PZN–PZT) ceramics with $Ba(W_{0.5}Cu_{0.5})O_3$ as the sintering aid that was manufactured in order to develop the low-temperature sintering materials for piezoelectric device applications. The phase transition, microstructure, dielectric, piezoelectric properties, and the temperature stability of the ceramics were investigated. The results showed that the addition of $Ba(W_{0.5}Cu_{0.5})O_3$ significantly improved the sintering temperature of PMN–PZN–PZT ceramics and could lower the sintering temperature from 1005 to 920 °C. Besides, the obtained $Ba(W_{0.5}Cu_{0.5})O_3$-doped ceramics sintered at 920 °C have optimized electrical properties, which are listed as follows: (K_p = 0.63, Q_m = 1415 and d_{33} = 351 pC/N), and high depolarization temperature above 320 °C. These results indicated that this material was a promising candidate for high-power multilayer piezoelectric device applications.

1. Introduction

Lead based piezoelectric ceramics have been extensively studied because of their favorable characteristics [1–3]. They are currently widely used in motors, piezoelectric actuators, piezoelectric transformers, ultrasonic vibrator, filter, blue luminescence and resonator, and medical applications [4,5]. For high-power multilayer piezoelectric device applications, piezoelectric materials are electrically driven to high mechanical vibration near the resonance frequencies, leading to a temperature rising and deterioration of piezoelectric properties with the increase of their vibration velocities [6,7]. Therefore, the lead-based piezoelectric ceramics should have high piezoelectric constant (d_{33}), high electromechanical coupling factor (K_p), high mechanical quality factor (Q_m), and good temperature stability [8,9].

However, PZT based ceramics have too high sintering temperature that is above 1200 °C, which induces evaporation of PbO during the sintering process [10]. Therefore, low temperature sintering of materials with maintaining the excellent piezoelectric properties is desirable for the use of high-electrical conductivity Ag metals as internal electrodes in order to reduce the cost during the fabrication process, which can cause serious pollution on the environment during the sintering process [11]. Furthermore, low-temperature sintering has many other advantages such as the compatibility with low temperature co-fired ceramics (LTCCs) and less energy consumption [12]. Therefore, the lead-based piezoelectric ceramics should also have low sintering temperature [13].

In our previous report, it was found that 0.10 wt.% ZnO–Li_2CO_3 and 2.0 wt.% Pb_3O_4 added PMN–PZN–PZT ceramics exhibited excellent piezoelectricity which was promising for the high-power piezoelectric device applications [14]. But the sintering temperature at 1005 °C was considerably relatively high for multilayered piezoelectric devices. In this study, the novel sintering aid $Ba(W_{1/2}Cu_{1/2})O_3$ was selected and was used to lower the sintering temperature of PMN–PZN–PZT ceramics by investigating the effects of $Ba(W_{1/2}Cu_{1/2})O_3$ addition on the sintering behavior, the phase structure, dielectric, piezoelectric properties and temperature dependence of PMN–PZN–PZT ceramics.

2. Experimental procedures

The ceramics were synthesized by solid state reaction method. The compositions are as follows:

$Pb(Mg_{1/3}Nb_{2/3})O_3$–$Pb(Zn_{1/3}Nb_{2/3})O_3$–$Pb(Zr_{0.52}Ti_{0.48})O_3$ (PMN–PZN–PZT) + 0.01 wt.% ZnO–Li_2CO_3 + 0.10 wt.% Pb_3O_4 + x wt.% $Ba(W_{1/2}Cu_{1/2})O_3$ (x = 0.00, 0.05, 0.13, 0.20, 0.25). The starting materials were Pb_3O_4 (97%), ZrO_2 (99%), TiO_2 (98%), ZnO (99%), Nb_2O_5 (99.5%), $MgCO_3$ (96.2%), Li_2CO_3 (99.5%), CuO (99.5%), WO_3 (99.9%), $BaCO_3$ (99%). In the first stage, CuO, $BaCO_3$ and WO_3 were

* Corresponding author at: School of Chemistry and Materials Science, Shaanxi Normal University, Xi'an 710062, Shaanxi, PR China. Tel.: +86 29 8531 0352; fax: +86 29 8530 7774.
E-mail address: yangzp@snnu.edu.cn (Z. Yang).

0925-8388/$ – see front matter © 2010 Elsevier B.V. All rights reserved.
doi:10.1016/j.jallcom.2010.09.085

thoroughly mixed in the stoichiometric ratio, and then calcined at 730 °C for 3 h to form $Ba(W_{1/2}Cu_{1/2})O_3$ with pure phase. In the second stage, the sintering aid was mixed in the stoichiometric ratio with other starting materials. Those materials were mixed by ball-milling in ethanol for 12 h using zirconium balls. The mixed powders were dried and calcined at 840 °C for 2 h in air. After calcination, the powders were pressed into disks with 15 mm diameter and 1.5 mm thickness under 100 MPa using the solution of polyvinyl alcohol as a binder. Through a 500 °C binder burnout, the samples were sintered at 900–950 °C for 4 h. At 850 °C, fired-on silver was printed on both sides for the electrodes. Then the samples were poled at 120 °C under a dc electric field of 3 kV/mm for 30 min in silicone oil.

The microstructure of the sintered bodies was observed using a scanning electron microscope (SEM Model Quanta200, FEI Company). The calcined powders and the sintered ceramics were examined by X-ray diffractometry (XRD Model DMX-2550/PC, Rigaku, Japan) to determine the crystalline phase at room temperature. Dielectric properties were obtained using an LCR meter (HP4294A) by measuring the capacitance from room temperature to 400 °C at 1 kHz. The piezoelectric constant (d_{33}) was measured using a quasi-static piezoelectric d_{33} meter (Model ZJ-3d, Institute of Acoustics Academic Sinica, China).

3. Results and discussion

Fig. 1 shows the XRD pattern (Fig. 1(a)) and c/a ratio (Fig. 1(c)) variation of specimens sintered at 920 °C as a function of $Ba(W_{1/2}Cu_{1/2})O_3$ content. If not considering the monoclinic phase at room temperature [15], it can be seen apparently that a pure perovskite structure without any secondary phases is confirmed by Fig. 1(a). The presence of diffraction peaks can be used to evaluate the structural order at long range or periodicity of the material as demonstrated [16]. PMN–PZN–PZT phase was confirmed by the comparison between the XRD patterns with the respective Joint Committee on Power Diffraction Standards (JCPDS) card No. 50-0346. All diffraction peaks can be assigned to the perovskite structure. PMN–PZN–PZT ceramics exhibited characteristic diffraction peaks correspondent to an ordered structure at long range. Typical rhombohedral phase is observed at room temperature when the $Ba(W_{1/2}Cu_{1/2})O_3$ content is 0.00 wt.%. The $(2\,0\,0)_R$ peak split into the $(0\,0\,2)_T$ and $(2\,0\,0)_T$ peaks with increasing $Ba(W_{1/2}Cu_{1/2})O_3$ content. The tetragonal phase can be obtained when $Ba(W_{1/2}Cu_{1/2})O_3$ content is above 0.05 wt.%. The crystal structure of the specimens changes profoundly by the addition of $Ba(W_{1/2}Cu_{1/2})O_3$. Rhombohedral and tetragonal phase coexists with $Ba(W_{1/2}Cu_{1/2})O_3$ content between 0.05 and 0.13 wt.%, demonstrating that the ceramic lies at the morphotropic phase boundary (MPB) [17]. The structure of solid solution transforms from rhombohedral phase to tetragonal phase due to the large distortion caused by $Ba(W_{1/2}Cu_{1/2})O_3$ addition. The lattice parameters of all samples are calculated by the program *UnitCell* [18]. Fig. 1(c) shows c/a ratio of specimens sintered at 920 °C as a function of $Ba(W_{1/2}Cu_{1/2})O_3$ content. The c/a ratio increases with increasing $Ba(W_{1/2}Cu_{1/2})O_3$ content. This may be due to the fact that $Ba(W_{1/2}Cu_{1/2})O_3$ ceramics with the low melting point is considered to form a complete solid solution and lead to the distortion of crystal lattice. The addition of $Ba(W_{1/2}Cu_{1/2})O_3$ solid solution promotes the substitution of the A and/or B site of the perovskite structure more effectively than the addition of raw metal oxides, increases structure defect and decreases the barrier among domains. It can be noted that the formation of $Ba(W_{1/2}Cu_{1/2})O_3$ solid solution is beneficial for the diffusion of ions and lower the sintering temperature of the ceramics.

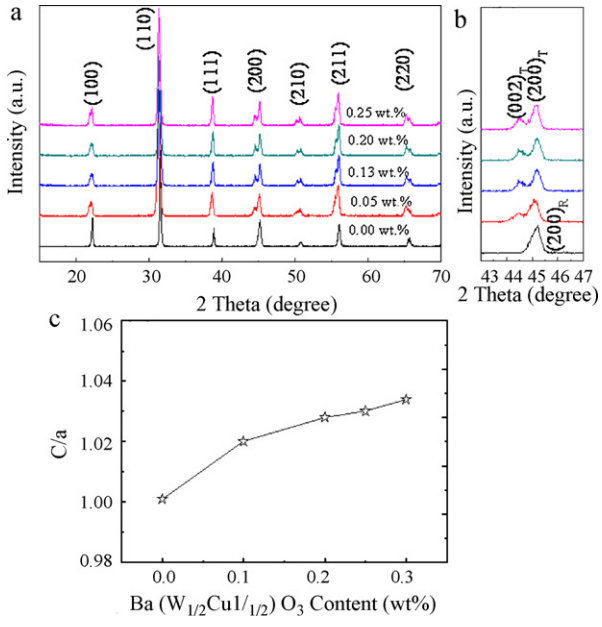

Fig. 1. XRD patterns and the c/a ratio variations of specimens sintered at 920 °C as a function of $Ba(W_{1/2}Cu_{1/2})O_3$ content.

Fig. 2 displays SEM micrographs of PMN–PZN–PZT ceramics sintered at 920 °C as a function of $Ba(W_{1/2}Cu_{1/2})O_3$ content. It can be seen from Fig. 3(a) that the microstructure is inhomogeneous and many distinct pores exist in the grain boundary for undoped specimens. As $Ba(W_{1/2}Cu_{1/2})O_3$ content is increased up to 0.13 wt.%, the grain size increases. The essential element of reactive liquid-phase sintering is the presence of a low-temperature liquid phase that must be able to directly or indirectly accelerate a reaction with the matrix phase. The reaction rate would increase when the reactants would dissolve in the liquid phase and the product would precipitate. The next important element of reactive liquid-phase sintering is the nature of the reaction with the matrix phase. The reaction must enhance mass-transport process, which are dominant in such a system during sintering. The formation of $Ba(W_{1/2}Cu_{1/2})O_3$ solid solution is beneficial to the ion lattice-diffusion. The lattice-diffusion coefficient is proportional to the vacancy concentration; as a result, the sintering rate will increase when the structural vacancies are generated during the reaction with the matrix phase. The process called a liquid-phase(-assisted) sintering, where the mass transport goes through the liquid phase by a solution-precipitation method, also promotes the sintering. This process can be further accelerated by an increase in the solubility of the matrix phase during or after the reaction. Finally, if during the reaction with the matrix phase a temporary or permanent amorphization occurs a viscous flow from the grain surface to the necks between the grains contributes to the sintering [19]. However, as $Ba(W_{1/2}Cu_{1/2})O_3$ content increases to 0.25 wt.%, the grain size decreases. This may be due to excess of 0.13 wt.% $Ba(W_{1/2}Cu_{1/2})O_3$ or only one of the additives accumulated at the grain boundaries, which inhibit the grain growth.

Fig. 3 shows piezoelectric constant (d_{33}), electromechanical coupling factors (K_p), and mechanical quality factor (Q_m) of specimens sintered at 920 °C as functions of $Ba(W_{1/2}Cu_{1/2})O_3$ content. SEM picture of specimens with 0.13 wt.% $Ba(W_{1/2}Cu_{1/2})O_3$ content sintered at 920 °C is inserted in Fig. 2(b). Values of d_{33}, K_p and Q_m increase with the increase of $Ba(W_{1/2}Cu_{1/2})O_3$ content, and the maximum values are obtained at 0.13 wt.%. The achievement of optimal values is mostly caused by the presence of a morphotropic phase boundary (MPB). The improvement of the dielectric and piezoelectric properties of the ceramics by adding 0.13 wt.% $Ba(W_{1/2}Cu_{1/2})O_3$ content is also probably caused by the presence of a homogeneous microstructure and well-grown grain in Fig. 2(b). We believe that these morphological characteristics are governed by the matter transport mechanism between the grains during the sintering process [20]. In this process, the grain boundaries play a fundamental role in the material transport into the system. The formation of large grains with irregular shapes could be a result of the variations on the kinetics of movement from boundary to boundary, since the grain-boundary energy is dependent on the grain-boundary orientation and grain-boundary

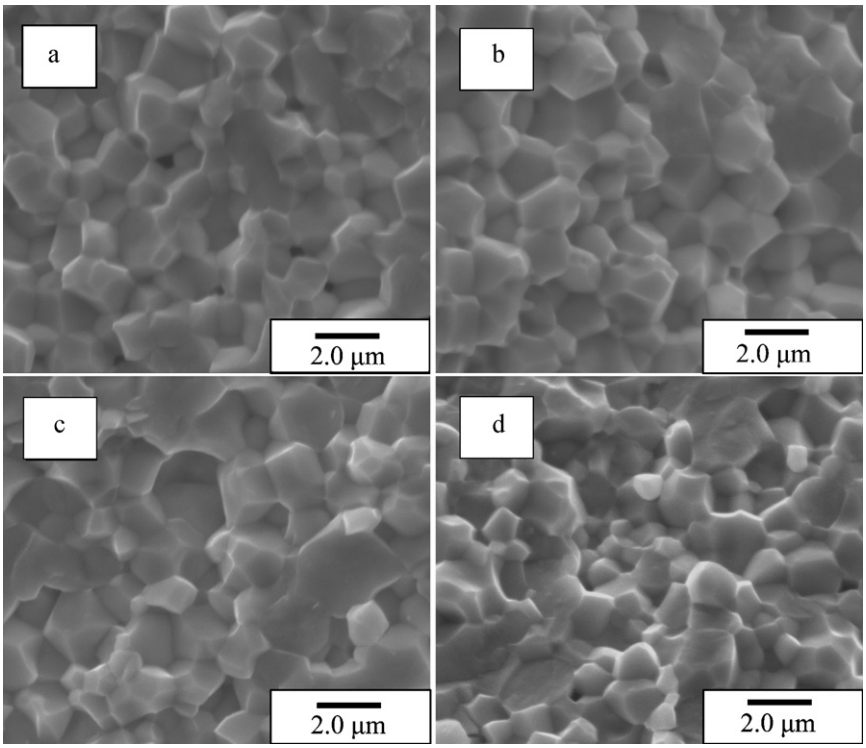

Fig. 2. SEM micrographs of PMN–PZN–PZT ceramics sintered at 920 °C as a function of $Ba(W_{1/2}Cu_{1/2})O_3$ content: (a) 0.00 wt.%; (b) 0.13 wt.%; (c) 0.20 wt.%; (d) 0.25 wt.%.

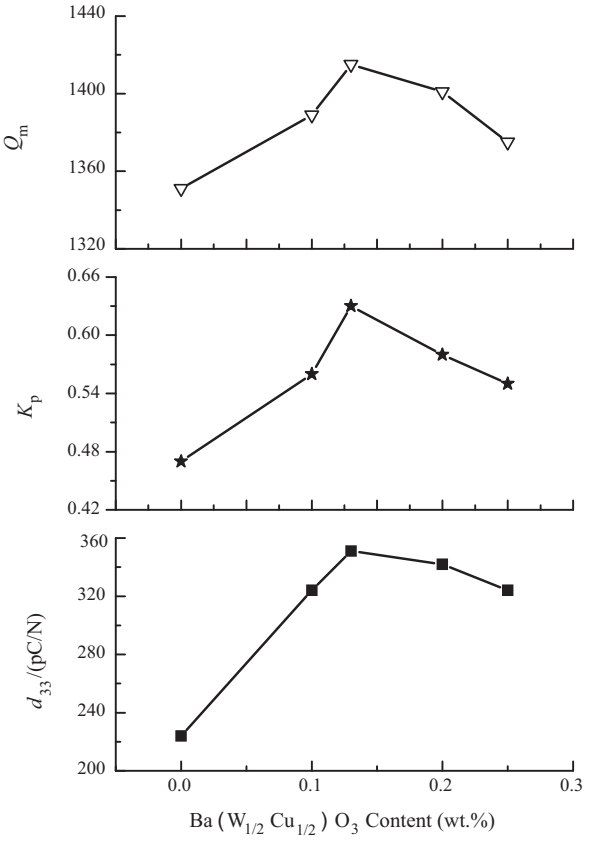

Fig. 3. d_{33}, K_p and Q_m of specimens sintered at 920 °C as functions of $Ba(W_{1/2}Cu_{1/2})O_3$ content.

mobility [21–23]. When the sintering process was performed at 920 °C for 4 h, the grain growth process was intensified, causing a reduction in the number of pores and disappearing with some grains, generally the smaller ones, a homogeneous microstructure and well-grown grain [24,25]. Table 1 shows the electrical properties of $Ba(W_{1/2}Cu_{1/2})O_3$-doped PMN–PZN–PZT ceramics. As can be seen from Table 1, with the increasing sintering temperature, d_{33}, K_p, Q_m and the dielectric constant (ε_r) increase. But when the sintering temperature is beyond 920 °C, a decrease of d_{33}, K_p, Q_m and ε_r after the maximum value is illustrated, which is caused by over addition and the increase of porosity due to over firing. Dielectric loss ($\tan\delta$) and ε_r show an opposite tendency approximately. As a result, 0.13 wt.% $Ba(W_{1/2}Cu_{1/2})O_3$-doped PMN–PZN–PZT ceramics sintered at 920 °C has the optimal values of d_{33}, K_p, Q_m, ε_r and $\tan\delta$, which are 351 pC/N, 0.63, 1415,1023 and 0.0078, respectively.

As we know, ionic radius of Pb^{2+} (1.49 Å) ion is close to that of Ba^{2+} (1.34 Å), so Ba^{2+} ion may replace Pb^{2+} ions in the A sites of ABO_3 perovskite structure. The substitution cannot change the charge neutrality. The difference of the two ions would result in a lattice distortion, and this is beneficial to lattice restoration and polarization of the material, which improves the intrinsic piezoelectric properties of the ceramics. For W^{5+} and Cu^{2+}, the ionic radii ($r_{W^{5+}} = 0.62$ Å and $r_{Cu^{2+}} = 0.72$ Å) are too small to enter into the A site. Since their ionic radii are similar to those of Zr^{4+} and Ti^{4+} ($r_{Zr^{4+}} = 0.79$ Å and $r_{Ti^{4+}} = 0.68$ Å), W^{5+} and Cu^{2+} prefer to enter into B site of ABO_3 structure. Whereas, the ionic radii of W^{5+} and Cu^{2+} ions are smaller than that of Zr^{4+} and Ti^{4+} ions. It is easy for them to enter into the crystal lattice and lead to the imbalance position which is also in favor of the enhancement of spontaneous polarization. The extra positive charges are introduced into the lattice due to the fact that the valent value of W^{5+} ion is higher than Zr^{4+}/Ti^{4+} ions. In order to maintain the charge neutrality, the increasing lead vacancies could generate electrons by ionization; most of the holes from lead vacancies are compensated by electrons. The following reactions summarize a postulated reasonable mechanism:

Table 1
The electral properties of $Ba(W_{1/2}Cu_{1/2})O_3$-doped PMN–PNN–PZT ceramics.

Sintering temperature (°C)	Content (wt.%)	d_{33} (pC/N)	K_p	Q_m	tan δ	ε_r	Sintering temperature (°C)	Content (wt.%)	d_{33} (pC/N)	K_p	Q_m	tan δ	ε_r
	0.00	211	0.37	1194	0.0105	801		0.00	224	0.47	1351	0.0102	809
	0.05	292	0.49	1211	0.0097	841		0.05	324	0.56	1389	0.0085	981
890	0.13	320	0.55	1254	0.0086	878	920	0.13	351	0.63	1415	0.0078	1023
	0.20	327	0.51	1232	0.0092	859		0.20	342	0.58	1401	0.0081	1007
	0.25	320	0.44	1108	0.0099	821		0.25	324	0.55	1375	0.0096	993
	0.00	264	0.50	1468	0.0099	858		0.00	288	0.59	1528	0.0092	901
	0.05	317	0.54	1362	0.0086	978		0.05	302	0.45	1195	0.0094	853
950	0.13	335	0.61	1396	0.0080	980	980	0.13	325	0.50	1257	0.0081	892
	0.20	328	0.56	1384	0.0086	939		0.20	315	0.49	1218	0.0085	862
	0.25	306	0.50	1335	0.0097	908		0.25	288	0.42	1144	0.0097	833

A W^{5+} ion gives birth to lead vacancies, which is listed as follows:

$$0.01WO_3 + Pb(Zr, Ti)O_3 \rightarrow (Pb_{0.99}V''_{Pb0.01})(Zr, Ti)_{0.99}W_{0.01}O_3 + PbO \uparrow$$

Otherwise, a Cu^{2+} ion gives birth to oxygen vacancies, which is listed as follows:

$$0.01CuO + Pb(Zr, Ti)O_3 \rightarrow Pb(Zr, Ti)_{0.99}Cu_{0.01}V_{O0.01}O_3 + 0.01(Zr, Ti)O_2$$

The appearance of lead vacancies and oxygen vacancies and the distortion of crystal lattice by W^{5+} and Cu^{2+} ions substituted for Zr^{4+}/Ti^{4+} ions facilitate the motion of domain walls resulting in a shift of domain states in the lattice. The increase of lead vacancies could generate electrons by ionization; most of the holes from lead vacancies are compensated by electrons from the donor level to make resistivity of PZT increased with the addition of donor dopants. As a result of higher resistivity, PZT piezoceramics are easily poled to facilitate the domain motion reoriented. And increasing of $Ba(W_{1/2}Cu_{1/2})O_3$ in the PMN–PZN–PZT lattice causes domain reorientation, thereby decreases Q_m and increases d_{33} and K_p. It is also well known that the electromechanical properties of PMN–PZN–PZT depend strongly on additives (nature and amount of dopant concentrations) as well as the MPB. The multiple ions (Li^+, Zn^{2+}, Cu^{2+}, etc.) occupying A and B-sites of the PMN–PZN–PZT lattice with the balance between charge and vacancies in the crystal lattice could result in enhanced piezoelectric properties.

In order to prevent the depolarization in the operating temperature range of the piezoelectric devices, the high T_c of 250 °C or higher is needed for piezoelectric materials [26]. Fig. 4(a) shows T_c of specimens as a function of $Ba(W_{1/2}Cu_{1/2})O_3$ content. It can be seen that T_c increases with increasing $Ba(W_{1/2}Cu_{1/2})O_3$ content at first. The maximum T_c value (322 °C) is obtained at 0.13 wt.% $Ba(W_{1/2}Cu_{1/2})O_3$ content. It is important that the stability and reliability of piezoelectric ceramics can be improved. The properties of piezoelectric devices, especially those working under high stress and high field, usually exhibit obvious degradation during their lifetime. Therefore, the depolarization temperature plays an important role in device applications [27]. Temperature dependence of d_{33} of PMN–PZN–PZT ceramics sintered at 920 °C with 0.13 wt.% $Ba(W_{1/2}Cu_{1/2})O_3$ content is shown in Fig. 4(b). The piezo-

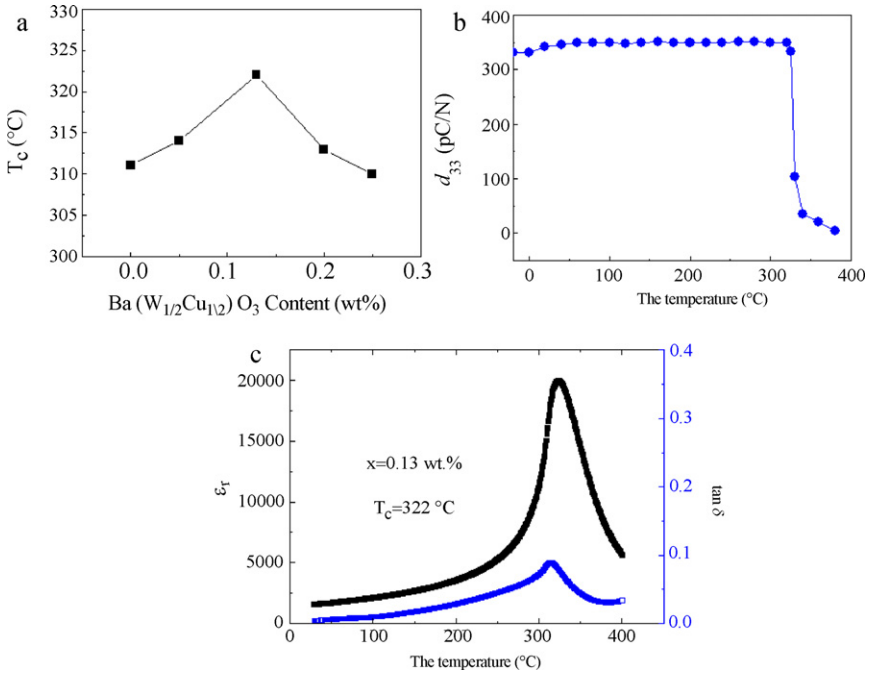

Fig. 4. T_c of specimens as a function of $Ba(W_{1/2}Cu_{1/2})O_3$ content, temperature dependence of d_{33} of PMN–PZN–PZT ceramics sintered at 920 °C with 0.13 wt.% $Ba(W_{1/2}Cu_{1/2})O_3$ content and temperature dependence of dielectric constant of PMN–PZN–PZT ceramics sintered at 920 °C with 0.13 wt.% $Ba(W_{1/2}Cu_{1/2})O_3$ content at 1 kHz.

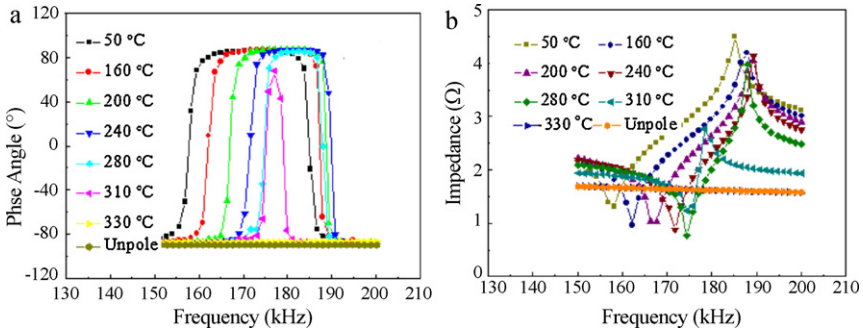

Fig. 5. The phase angle θ and impedance Z of the samples as a function of frequency and the various temperatures.

electric constant slightly changes with temperature increasing to 320 °C, and then significantly decreases with further increase in temperature. The temperature at which the piezoelectric responses obviously degrade is about 320 °C. That is, the depolarization temperature of the ceramics is about 320 °C. Fig. 4(c) displays temperature dependence of dielectric constant of PMN–PZN–PZT ceramics sintered at 920 °C with 0.13 wt.% $Ba(W_{1/2}Cu_{1/2})O_3$ content at 1 kHz. It can be seen from Fig. 3(c) that the Curie temperature of 322 °C is obtained. This Curie temperature is high enough to contribute to the general stability of material characteristics for multilayer piezoelectric transformer applications during operation process [28].

Fig. 5 shows the phase angle θ and impedance as functions of frequency and temperatures for 0.13 wt.% $Ba(W_{1/2}Cu_{1/2})O_3$-doped specimens sintered at 920 °C. Fig. 4(a) shows that under the ideal poling state, θ will have a value of 90° in the frequency range between the anti-resonance and resonance frequencies [29]. The observed θ for $Ba(W_{1/2}Cu_{1/2})O_3$-doped specimens is 89°, indicating that it is easier to pole the ceramics to the ideal state. It can be seen in Fig. 4(a) that the frequency bandwidth Δf ($\Delta f = f_a - f_r$) decreases with increase in the temperature, and it vanishes when the temperature is close to 330 °C. θ becomes constant ($\approx -89.9°$) at the same time. The result shows the same trend of the phase angle θ of the unpoled sample, as shown in Fig. 4(a). In Fig. 4(b), the anti-resonant frequencies (f_a) decrease with the increasing temperature, and the trend is reversed for resonant frequency (f_r). This phenomenon is related to the increased domain activities and defect pinning by spaces charges at higher measured temperatures. The explanation of the temperature dependence of fatigue should consider both domain states and space-charge mobility at different temperatures. At lower temperature below T_c, fewer domain walls are available for pinning so that the extrinsic contribution of domain walls to the piezoelectric response is small. At higher temperatures near T_c, the lower fatigue rates could primarily be contributed by the decrease of the polarization in the samples, since the domains or defects which have been pinned by space charges could be depinned by the AC field. At temperatures above T_c, the ferroelectric phase has been translated to the paraelectric phase wherein the spontaneous polarization disappeared and all the domains no longer exist causing decrease in piezoelectric constant d_{33} [30]. Furthermore, the Δf becomes smaller by increasing the temperature. As seen from $K_p = \left[2.51 \times (f_a - f_r) f_r^{-1}\right]^{1/2}$, a smaller Δf can be used to elucidate the rapid decrease in K_p value when the measured temperature increases and approaches to the T_c. The frequency dependence of impedance of the sample at temperature of 320 °C is similar to that of an unpoled sample in Fig. 4(b). The results show that the depolarization temperature of the ceramics is above 320 °C, and the ceramics show good temperature stability in temperature range from room temperature to 320 °C. The changes in Fig. 4 are in accordance with the changes in Fig. 3.

4. Conclusions

The PMN–PZN–PZT ceramics doped with $Ba(W_{1/2}Cu_{1/2})O_3$ were fabricated by conventional ceramic techniques. The results indicate that the crystalline symmetry changes from the rhombohedral phase to the tetragonal phase with increasing $Ba(W_{1/2}Cu_{1/2})O_3$ contents. The phase changes are attributed to the form of $Ba(W_{1/2}Cu_{1/2})O_3$ solid solution with the low melting point. It leads to the distortion of crystal lattice, promotes the substitution of the A and/or B site of the perovskite structure, increases structure defect and decreases the barrier among domains. It can be noted that the formation of $Ba(W_{1/2}Cu_{1/2})O_3$ solid solution is beneficial for the diffusion of ions and lower the sintering temperature of the ceramics. The addition of $Ba(W_{1/2}Cu_{1/2})O_3$ not only decreases the sintering temperature from 1005 to 920 °C, but also optimizes the properties of the ceramics. 0.13 wt.% $Ba(W_{1/2}Cu_{1/2})O_3$-doped PMN–PZN–PZT ceramics sintered at 920 °C exhibits excellent room temperature electrical properties, which are listed as follows: $d_{33} = 351$ pC/N, $K_p = 0.63$, $Q_m = 1415$, $\varepsilon_r = 1023$ and $\tan\delta = 0.0078$ and $T_c = 322$ °C. The achievement of optimal values is attributed to the presence of a morphotropic phase boundary (MPB) and a homogeneous microstructure and well-grown grain. These microstructural characteristics are attributed to the matter transport mechanisms via grain boundary during the low sintering process. Besides, the electromechanical properties keep stable in a wide temperature range from room temperature to 320 °C. The optimal electrical properties and the favorable temperature stability make 0.13 wt.% $Ba(W_{1/2}Cu_{1/2})O_3$ doped PMN–PZN–PZT ceramics to be promising candidate for multilayer piezoelectric device applications.

Acknowledgements

This work was supported by National Science Foundation of China (NSFC) (Grant No. 20771070), Natural Science Research Program of Shaanxi Province (Grant No. 2009JZ003) and Supported by the Fundamental Research Funds for the Central Universities.

References

[1] H. Hao, S.J. Zhang, H.X. Liu, R. Thomas Shrout, J. Appl. Phys. 105 (2009) 024104.
[2] J.Y. Ha, J.W. Choi, C.Y. Kang, D.J. Choi, H.J. Kim, S.J. Yoon, Mater. Chem. Phys. 90 (2005) 396.
[3] J.S. Cross, K. Shinozaki, T. Yoshioka, J. Tanaka, S.H. Kim, H. Morioka, K. Saito, Mater. Sci. Eng. B 173 (2010) 18.
[4] Y. Fang, Y. Xiong, Y.L. Zhou, J.X. Chen, et al., Solid State Sci. 11 (2009) 1131.
[5] A. Phuruangrat, T. Thongtem, S. Thongtem, J. Cryst. Growth 311 (2009) 4076.
[6] G.Z. Wang, G.P. Wan, J. Alloys Compd. 484 (2009) 505.
[7] F.F. Popescu, V. Bercu, J.N. Barascu, et al., Opt. Mater. 32 (2010) 570.
[8] M. Tyagi, Sangeeta, D.G. Desai, S.C. Sabharwal, J. Lumin. 128 (2008) 22.
[9] Y. Cheng, Y. Yang, Y.P. Wang, H.Q. Meng, J. Alloys Compd. (2010), doi:10.1016/j.jallcom.2010.12.115.
[10] X.L. Chao, D.F. Ma, R. Gu, Z.P. Yang, J. Alloys Compd. 491 (2010) 698.
[11] H.L. Du, Z.B. Pei, W.C. Zhou, F. Luo, S.B. Qu, Mater. Sci. Eng. A 421 (2006) 286.

[12] X. Hao, Z. Zhang, J. Zhou, S. An, J. Zhai, J. Alloys Compd. 501 (2010) 358.
[13] S. Rattanachan, Y. Miyashita, Y. Mutoh, Int. J. Fatigue 28 (2006) 1413.
[14] X.L. Chao, Z.P. Yang, G. Li, Y.Q. Chen, Sens. Actuators A: Phys. 144 (2008) 117.
[15] K. Kakegawa, O. Masunaga, J. Am. Ceram. Soc. 78 (1995) 1071.
[16] L.S. Cavalcante, V.S. Marques, et al., Chem. Eng. J. 143 (2008) 299–307.
[17] S. Kaneko, D.Z. Dong, K. Murakami, J. Am. Ceram. Soc. 81 (1998) 1013.
[18] T.J.B. Holland, S.A.T. Redfern, Miner. Mag. 61 (1997) 65.
[19] V. Mtjaz, S. Danilo, O. Sugiyama, et al., J. Eur. Ceram. Soc. 26 (2006) 2777.
[20] T. Badapanda, S.K. Rout, et al., J. Phys. D: Appl. Phys. 42 (2009) 175414.
[21] M. Kakihana, J. Sol–Gel Sci. Technol. 6 (1960) 7.
[22] M.N. Rahaman, Sintering of Ceramics, CRC Press (Taylor and Francis Group), Boca Raton, FL, 2008, pp. 55–106.
[23] S.J.L. Kang, Sintering-Densification, Grain Growth and Microstructure, Elsevier, Amsterdam, 2005, pp. 39–91.
[24] A. Ramasubramaniam, V.B. Shenoy, Acta Mater. 53 (2005) 2943.
[25] S.B. Reddy, K.P. Rao, M.S.R. Rao, J. Alloys Compd. 481 (2009) 692.
[26] D. Liua, Y.Y. Zhang, W. Wang, B. Rena, Q.H. Zhang, J. Jiao, X.Y. Zhao, H. Luo, J. Alloys Compd. 481 (2009) 692.
[27] S.K. Pandey, O.P. Thakur, A. Kumar, C. Prakash, R. Chatterjee, T.C. Goel, J. Appl. Phys. 506 (2010) 428.
[28] W.P. Chena, H.L.W. Chan, F.C.H. Yiu, K.M.W. Ng, P.C.K. Liu, Appl. Phys. Lett. 80 (2002) 19.
[29] A. Moure, C. Alemany, L. Pardo, IEEE Trans. Ultrasonic Ferr. 52 (2005) 570.
[30] Q.Y. Jiang, E.C. Subbarao, L.E. Cross, J. Appl. Phys. 75 (1994) 7433.